ORGANIC CHEMISTRY FRONTIERS

RESEARCH ARTICLE

View Article Online
View Journal | View Issue

Cite this: *Org. Chem. Front.*, 2025, **12**, 430

Influence of hydrogen bonds and π–π stacking on the self-assembly of aryldipyrrolidones†

Pedro Ximenis,[a] Llorenç Rubert,[a] Heike M. A. Ehmann[b] and Bartolome Soberats *[a]

Received 24th August 2024,
Accepted 9th November 2024

DOI: 10.1039/d4qo01577k

rsc.li/frontiers-organic

We report on the self-assembly behaviour in solution and in the solid-state of two newly designed bis-dendronized aryldipyrrolidone (**BDP** and **NDP**) dyes with two free N–H groups at the lactam positions. Interestingly, while the naphthalene-based **NDP** self-assembles *via* π–π-stacking to form conventional columnar liquid-crystalline (LC) assemblies, the smaller benzene-based **BDP** forms unconventional columnar LC phases with the dyes parallel to the columnar axis, *via* hydrogen-bonding interactions. This work presents new design principles to modulate hydrogen bonding in dye materials with potential application in optoelectronics.

Introduction

Discotic liquid crystals have attracted significant attention due to their optical properties and potential applications in optoelectronics.[1–5] These materials usually consist of π-conjugated chromophores (or dyes) functionalized with long alkyl chains at their periphery. Importantly, molecular engineering of these discotic liquid crystals has become a powerful tool to fine-tune the spatial interactions between liquid crystal molecules, thereby modulating their packing, exciton coupling, and properties.[6–11] In this context, discotic liquid crystal molecules typically self-assemble *via* co-facial π–π interactions, forming columnar structures in which the chromophores are oriented perpendicular to the columnar axis.[1–11] This arrangement generally results in H-type aggregates,[12,13] which function well as semiconductors and have been successfully applied in electronic devices,[14–16] including solar cells,[17] OLEDs,[18] and OFETs.[19]

Recently, a novel class of dye-based columnar liquid crystals was discovered, distinguished by the alignment of the chromophores with their π-conjugated cores parallel to the columnar axis.[20–25] Such unconventional organization was achieved through multiple hydrogen (H)-bonding interactions along the π-plane of the chromophores. For instance, a series of tetra-dendronized perylene bisimides (PBIs) were reported to form liquid-crystalline (LC) J-aggregates based on H-bonded PBI subunits, which further assemble into columns composed of multiple strands.[21] This unique columnar assembly mode has so far been reported in specially designed PBIs,[20–22] diketopyrrolopyrroles,[23,24] and naphthalene bisimides (NBI).[25] Notably, such assemblies can lead to the formation of J-aggregates,[20–22,25–28] which are typically challenging to achieve in LC columnar phases. Therefore, exploring these types of assemblies is of significant interest for the development of advanced photonic materials.[29,30]

During our investigations, we became interested in aromatic dipyrrolidones, a class of diketopyrrolopyrrole derivatives with great potential for the development of H-bonded dye materials.[31] For instance, aryldipyrrolidones are utilized to prepare highly conjugated polymers,[32–36] exhibiting excellent optoelectronic properties.[37,38] To enhance solubility, alkyl groups are often attached to the nitrogen atoms of the lactam units, while polymers with free N–H groups feature H-bonding capabilities.[36] To date, no supramolecular assemblies of low molecular weight aryldipyrrolidones have been reported in either the LC state or in solution.

Herein, we introduce two novel bisdendronized aryldipyrrolidones featuring benzene (**BDP**) and naphthalene (**NDP**) cores and free N–H groups at the lactam units (Fig. 1a), which have been designed to self-assemble *via* double self-complementary H-bonds (Fig. 1b). Both compounds were found to form columnar LC phases in bulk and supramolecular polymers in organic solvents. Interestingly, the **BDP** derivative self-organizes into a multistranded columnar LC phase *via* H-bonding interactions, with the aromatic cores aligning parallel to the columnar axis (Fig. 1d). However, the larger **NDP** derivative self-assembles through primary π–π interactions into conventional LC columnar stacks (Fig. 1d) with no H-bond contributions. The distinct self-assembly behaviour of these molecules is attributed to the larger π-core of **NDP**, which favours assembly *via* π–π stacking over H-bonding.[39–41] This study provides new insights into controlling the self-assembly of dyes in both solution and the LC state.

[a]*Department of Chemistry, Universitat de les Illes Balears, Cra. Valldemossa Km 7.5, 07122 Palma de Mallorca, Spain. E-mail: b.soberats@uib.es*
[b]*Anton Paar GmbH, Anton-Paar-Straße 20, 8054 Graz, Austria*

† Electronic supplementary information (ESI) available. See DOI: https://doi.org/10.1039/d4qo01577k

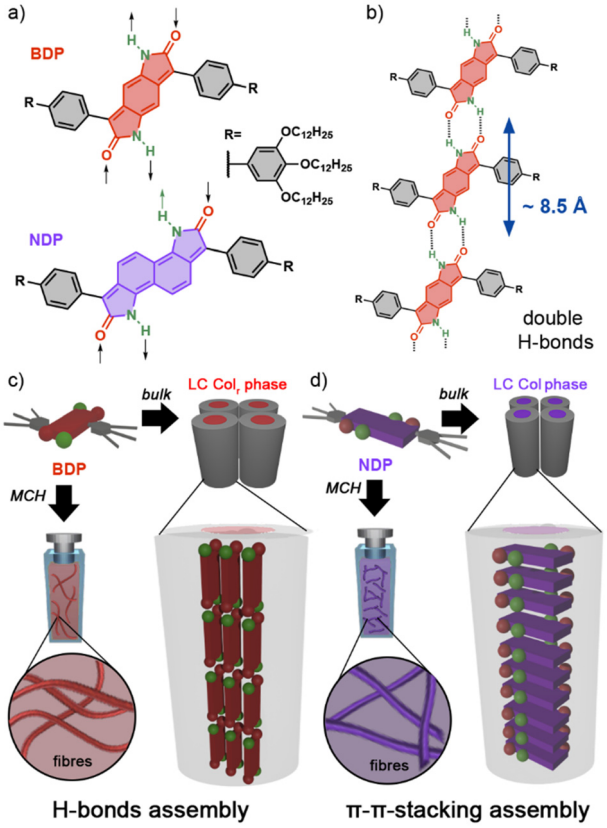

Fig. 1 (a) Molecular structures of the aryl dipyrrolidones **BDP** and **NDP**. Black arrows indicate the H-bonding donor–acceptor behaviour of the molecules. (b) Formation of complementary H-bonds between the **BDP** units. Scheme of the self-assembly features in bulk and in methylcyclohexane (MCH) of (c) **BDP** and (d) **NDP**. The dendron part in the cartoon has been omitted for clarity. Col_r: columnar rectangular LC phase; Col: columnar LC phase.

Results and discussion

Molecular design

The chemical structures of **BDP** and **NDP** consist of benzene and naphthalene cores symmetrically fused with two 2-pyrrolidone units, which are connected to phenyl-3,4,5-tridodecyloxyphenyl wedge-shaped moieties (Fig. 1a). These wedge-shaped components are expected to enhance solubility in organic solvents and confer LC properties,[23,24] while the central cores are known for their photoactive characteristics.[32–38] The π-extended nature of the **BDP** and **NDP** structures suggests a strong potential for π–π stacking interactions, while the unsubstituted N–H positions at the lactam units may enable the establishment of complementary H-bonds (Fig. 1b).[20–25]

NDP and **BDP** were synthesized by modifying previously reported methods,[32,36] yielding coloured waxy solids in moderate yields (see the ESI†). Both compounds demonstrated good solubility in organic solvents such as $CHCl_3$, tetrahydrofurane, and methylcyclohexane (MCH). In $CHCl_3$ solutions, **BDP** appeared orange and **NDP** blueish, with both exhibiting luminescence properties (Figs S7–S9†).

Studies in solution

To initially assess the self-assembly behaviour of **BDP** and **NDP**, we conducted aggregation studies in solution.[42–44] The supramolecular polymerization was monitored in MCH using UV/vis spectroscopy through temperature-dependent studies. At 363 K, **BDP** exhibited a strong absorption band with a maximum at 510 nm (Fig. 2a), corresponding to the monomeric species .[31–38] As the sample cooled down, this band underwent a hypsochromic shift from 510 nm to 482 nm, accompanied by a decrease in the absorption intensity (Fig. 2a), which was attributed to an aggregation process. The blueshift of the absorption maximum upon aggregation suggests the formation of an H-type aggregate.[12,13] Similarly, **NDP** displayed the main absorption band peaking at 597 nm at 363 K, indicative of the monomeric state. Upon cooling, this absorption band also showed a blueshift, signalling the polymerization process and the formation of an H-aggregate.

For both compounds, the fraction of aggregated species (α_{agg}) was plotted against temperature at λ = 482 nm for **BDP** and at λ = 569 nm for **NDP** across various concentrations (Fig. 2a and b, S10 and S11†). The resulting plots displayed non-sigmoidal curves (Fig. 2c and d), suggesting that these compounds self-assemble through cooperative mechanisms.[45–47] Thermodynamic analysis of these plots

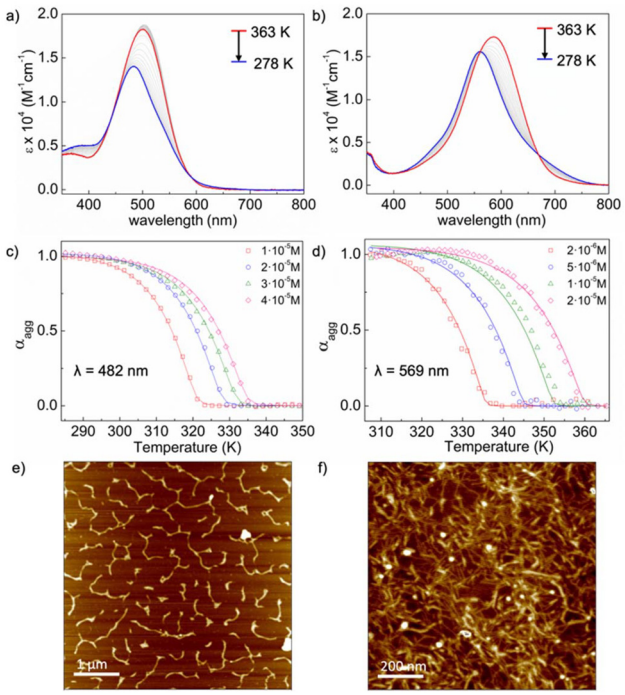

Fig. 2 Temperature-dependent UV/vis absorption spectra of (a) **BDP** (1 × 10^{-5} M, MCH) and (b) **NDP** (1 × 10^{-5} M, MCH) between 363 and 278 K (cooling cycles, 1 K min^{-1}). Plot of the experimental degree of aggregation (α_{agg}) over T (symbols) at different concentrations (MCH) for (c) **BDP** and (d) **NDP** and the corresponding fits according to the nucleation–elongation model (solid lines). (e) AFM image of a spin-coated solution of **BDP** in MCH (4 × 10^{-5} M) on a mica surface. (f) AFM image of a spin-coated solution of **NDP** in MCH (4 × 10^{-5} M) on a HOPG surface.

(Fig. 2c and d) further confirmed a nucleation–elongation mechanism for both **BDP** and **NDP**, with ΔG° values of −34.8 and −43.1 kJ mol^{-1}, respectively (Tables S1 and S2†).[48,49]

The morphologies of the aggregated species of **BDP** and **NDP** were investigated using atomic force microscopy (AFM) (Fig. 2e and f, S14 and S15†). MCH solutions of the corresponding aggregates were spin-coated onto mica or highly oriented pyrolytic graphite (HOPG) substrates and measured in tapping mode at room temperature (see the ESI† for details). As shown in Fig. 2e and f, both **BDP** and **NDP** aggregates exhibited fibrillar morphologies.[42–47] Both compounds tended to form fibrillar bundled species on HOPG surfaces (Fig. 2f and S17a†) while longer and thicker fibres are observed on mica (Fig. 2e), where dewetting effects may also take place. Nevertheless, AFM experiments clearly demonstrate the tendency of **BDP** and **NDP** to form 1D-assembled nanostructures in MCH solutions.

FT-IR analysis revealed that both **BDP** and **NDP** exhibited an N–H stretching vibration at 3448 cm^{-1} in $CHCl_3$ (Fig. S12 and S13†), indicating that the lactam N–H groups are not H-bonded in this solvent and probably both compounds are monomerically dissolved. In contrast, the N–H stretching vibration for **BDP** shifted to 3141 cm^{-1} in MCH-*d14* (Fig. S12b†), clearly indicating H-bond formation.[20–25,50] However, no N–H stretching signal was detected for **NDP** in MCH-*d14* (Fig. S13b†). Instead, the C=O stretching band of **NDP** was monitored and showed no significant changes in $CHCl_3$ and MCH-*d14* (Fig. S13†). This suggests that, unlike **BDP**, the **NDP** aggregate in MCH-*d14* is probably not formed by strong H-bonds.

To demonstrate the different assembly modes of **BDP** and **NDP**, we conducted additional UV-vis and NMR experiments. Denaturation UV-vis experiments using acetonitrile, a competitive H-bonding solvent, showed that the **BDP** aggregate is more susceptible to dissasemble by increasing amounts of acetonitrile than the **NDP** aggregate (Fig. S14†), suggesting that H-bonds play a more significant role in the assembly of **BDP**. However, these experiments revealed that both aggregates are relatively weak when exposed to polar solvents at 10^{-5} M concentrations. Temperature-dependent ^{1}H NMR studies were also conducted for both compounds at a concentration of 5×10^{-4} M in MCH (Fig. S15 and S16†). The ^{1}H NMR spectrum of **BDP** exhibited very broad peaks at lower temperatures, indicating a high degree of aggregation. Upon heating, the signals became sharper, and the NH peaks showed a shielding trend (Fig. S15†), suggesting the disassembly of the aggregate *via* rupture of H-bonds. In contrast, the ^{1}H NMR spectra of **NDP** showed almost no variation over the studied temperature range (Fig. S16 and S11e†), indicating that no significant disaggregation occurred. The superior stability of the **NDP** aggregate was attributed to an assembly mode primarily based on π–π interactions rather than H-bonds, as supported by the FT-IR and denaturation UV-vis studies (Fig. S12–S14†).

Liquid-crystalline behaviour

The LC behaviour of **NDP** and **BDP** was studied using polarizing optical microscopy (POM), differential scanning calorimetry (DSC), and wide-angle X-ray scattering (WAXS). Pleasingly, both compounds were found to show LC phases according to the POM and DSC analyses (Fig. S19–S22†), and the phase transition behaviour is shown in Table 1. **BDP** exhibits two enantiotropic LC phases (Fig. S21†) appearing between 202 and 153 °C, and between 153 and 45 °C, respectively, during the cooling cycle. Curiously, the **BDP** shows a second-order transition at around 45 °C, which was assigned to a glass transition process (Fig. S21†).[51] It is noteworthy that the sample showed gradual decomposition when kept at temperatures above 150 °C in open air.

Table 1 Phase transition behaviour of **BDP** and **NDP**

BDP	1st cooling	Iso 202 Col_h 153 Col_r 45[b] $Col_{r(SC)}$ −3 Cr
	2nd heating	Cr 4 $Col_{r(SC)}$ 50[b] Col_r 172 Col_h 204 Iso
NDP	1st cooling	240[a] Col_x 17 Cr
	2nd heating	Cr 24 Col_x 251 Iso (decomp.)

Transition temperatures are indicated in °C. [a] All transition temperatures were obtained from DSC experiments, except those that were obtained *via* POM observations. [b] Indicates a glass transition. Iso: isotropic; Col_h: columnar hexagonal; Col_r: columnar rectangular; $Col_{r(SC)}$: soft-crystalline columnar rectangular; Cr: crystalline; Col_x: unidentified columnar.

The structural features of the **BDP** LC phases were evaluated using wide-angle X-ray scattering (WAXS) on extruded fibres of the sample at 25, 80, and 190 °C.[20–25] The WAXS pattern at 80 °C (Fig. 3a) revealed two strong and five weak signals along the equator, which were identified as the 100, 010, 110, 200, 210, 020 and 310 reflections of a simple columnar rectangular (Col_r) phase with a = 33.6 Å and b = 26.2 Å (Fig. 3a and S27†).[1–11,52] This Col_r phase was found to persist at lower temperatures (25 °C) with only slight changes in the lattice parameters (a = 33.2 Å and b = 26.6 Å) (Table 1, Fig. S24 and S25†). Based on the high viscosity of this phase observed in POM studies, it was assumed that it corresponds to a glassy or a soft-crystalline columnar phase ($Col_{r(SC)}$).[53] In contrast, at 190 °C, the WAXS pattern of **BDP** fitted well with a more disordered columnar hexagonal (Col_h) phase, with a = 38.3 Å (Fig. S28 and S29†).

NDP, on the other hand, exhibits a single LC phase between 24 and 251 °C, after which the sample clears and decomposes (Fig. S20 and S22†).[23] The WAXS pattern of an aligned fibre of **NDP** at 80 °C revealed only an equatorial strong reflection at 46.3 Å besides the diffuse halo at 4.4 Å (Fig. 3b, S30 and S31†). Due to the low number of peaks, it was not possible to accurately assign this phase. However, considering the WAXS pattern (Fig. 3b), the POM texture consisting of small birefringent domains (Fig. S20†), as well as the molecular structure and the LC behaviour of the related molecules,[1,11,20–25] it is likely that **NDP** formed a columnar phase (Col_x), although more information cannot be obtained regarding the columnar organization from the WAXS experiments.

Anisotropic features and assembly mode

To gain a deeper understanding of the molecular packing within the columnar LC structures of **BDP** and **NDP**, we conducted

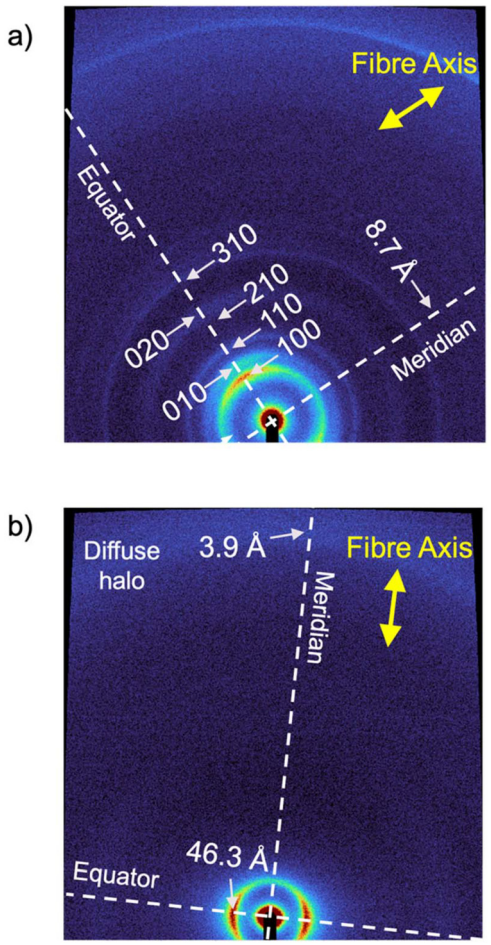

Fig. 3 WAXS patterns of extruded fibre of (a) **BDP** and (b) **NDP** at 80 °C. The directions of the fibre axes are indicated with yellow arrows.

additional experiments on aligned samples to analyse the anisotropic properties. In this line, we first analysed the anisotropic features of the WAXS patterns (Fig. 3) that were recorded using extruded fibres. The WAXS pattern of **BDP** at 80 °C displays a reflection on the meridian at 8.7 Å, which corresponds well with the molecular distance of the **BDP** core H-bonded through the 2-pyrrolidone groups (Fig. 1b). An analogous meridional signal was also found in the Col_h phase at 8.4 Å measured at 190 °C (Fig. S28). The observation of these meridional peaks is consistent with previous studies on related compounds,[20–25] and suggests that the **BDP** molecules are likely aligned with their π-cores along the columnar axis. Furthermore, we calculated the number of molecules per columnar stratum in the Col_r phase at 80 °C and in the Col_h phase at 190 °C, and it was found that these phases are composed of three and four molecules of **BDP** per ~8.5 Å slices (Tables S7 and S8†), respectively. This suggests that the columnar LC structures of **BDP** consist of multi-stranded assemblies of H-bonded dyes, similar to those reported for LC PBIs and NBIs.[20–22,25]

To confirm the orientation of the **BDP** molecules in the columnar LC phases, we conducted polarized experiments on mechanically sheared samples on different substrates. It is known that columnar liquid crystals can be macroscopically aligned by mechanical shearing, resulting in the columns being oriented along the shearing direction.[1–11,20–25] The successful alignment of **BDP** columnar phases on glass plates was confirmed using POM, which showed that the image becomes brighter when the polarizer and analyser are rotated 45° relative to the shearing direction (Fig. 4a), compared to when they are aligned parallel or perpendicular to it (Fig. 4b).[20–25] The polarized FT-IR spectrum of the sheared sample of **BDP** on a KBr plate showed that the N–H band appears at 3123 cm^{-1}, indicating H-bond formation.[20–25] More importantly, the N–H band was more intense when the polarizer is parallel to the shearing direction compared to when it is perpendicular (Fig. 4c). These results confirm that the benzenedipyrrolidone cores are aligned along the column axis, establishing H-bonds. Thus, we propose that **BDP** self-assembles into H-bonded strands, which then bundle together to form columnar structures composed of three (Col_r, 80 °C) (Fig. 1c) or four (Col_h, 190 °C) strands.[20–25] Importantly, the **BDP** molecules are positioned at the centre of the columns, parallel to the columnar axis, and are surrounded by alkyl chains. No anisotropic features were observed by polarized UV/vis experiments (Fig. S32†). However, the appearance of the absorption maximum at 500 nm confirms that the columnar LC **BDP** forms H-type couplings and therefore the molecules may stack in a co-facial manner, normal to the columnar axis, with no slipping between them, as shown in Fig. 1c.

On the other hand, the analysis of the WAXS pattern of the aligned fibre of **NDP** (Fig. 3b) showed no intense meridional peaks. However, a weak shoulder was observed at 3.9 Å (Fig. S31†), which was attributed to a repeating unit along the columnar axis, consistent with the cofacial assembly of **NDP** with a relatively long π-stacking distance.[2] To confirm the rela-

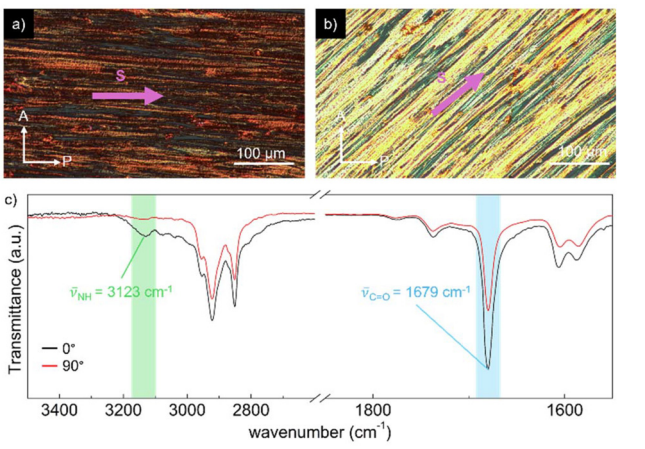

Fig. 4 POM images of a sheared sample of **BDP** on a glass plate with the instrument polarizer (P) (a) parallel to the shearing direction and (b) after 45° rotation of the sample holder. The direction of the shearing (S) is indicated with pink arrows. (c) FT-IR spectra of a sheared sample of **BDP** on a KBr plate with the polarizer parallel (black line) and perpendicular (red line) to the shearing direction. N–H and C=O stretching bands are shown in the inset.

tive orientation of the molecules in the Col_x LC phase, we carried out polarized experiments on aligned samples of **NDP** (Fig. S32, S33 and S35†). Curiously, no anisotropic behaviour was observed on the FT-IR experiment by the N–H or C=O stretching bands upon rotation of the polarizer (Fig. S35†). This observation suggested that the N–Hs are not oriented in any specific direction of the aligned sample. More importantly, the appearance of a very broad N–H stretching band centred at 3442 cm^{-1} was observed, which indeed indicates that no H-bonds are formed in the liquid crystal assembly. Based on this, the molecular shape with two dendrons, and the observation of a meridional WAXS signal at 3.9 Å, the most plausible assembly mode of the Col_x phase of **NDP** should be based on π–π interactions, as shown in Fig. 1d. This assumption aligns with the solution studies suggesting that **NDP** assembles *via* conventional stacking rather than H-bonds (Fig. S14b, S14c and S16†). However, no further details of the LC assembly could be determined due to the poor scattering of the sample.

According to these results, it is apparent that the **NDP** and **BDP** display a significantly different assembly modes in their columnar LC phases. While the **BDP** assembles by H-bonds into multistranded columnar phases,[20–25] **NDP** forms a more conventional packing based on co-facial interactions between the π-conjugated scaffold.[2] We hypothesize that this change in the assembly mode is driven by the increase on the π-surface in **NDP**, which significantly increase the ability of the molecules to interact by π–π-stacking.[39] Furthermore, it is possible that other steric effects arising between the dendrons may also play a role.[54]

Conclusions

In this study, we explored the self-assembly behaviour of two novel aryldipyrrolidones, **BDP** and **NDP**, as promising dyes with potential to form functional materials. These compounds are based on benzene (**BDP**) and naphthalene (**NDP**) cores, and both feature free N–H groups on their lactam units. Our investigations revealed that both compounds form columnar LC phases in bulk and supramolecular polymers in organic solvents. The **BDP** derivative displayed a unique self-organization into multistranded columnar LC phases driven by hydrogen bonding, with the aromatic cores aligned parallel to the columnar axis. In contrast, the **NDP** derivative, which possesses a larger π-core, self-assembles primarily through π–π interactions into conventional LC columnar stacks, with no significant contribution from hydrogen bonding. The distinct self-assembly behaviours observed between **BDP** and **NDP** highlight the influence of core size on the assembly process, where the larger π-core of **NDP** favours π–π stacking over hydrogen bonding. These findings provide new insights into the design and control of dye self-assembly in both solution and liquid-crystalline states, offering potential pathways for the development of advanced functional materials.

Author contributions

P. X. carried out the synthesis of the compounds and all the aggregation and characterization studies and contributed to manuscript preparation. L. R. contributed to the synthesis of **BDP** and the realization of the assembly experiments. H. M. A. E. performed the WAXS experiments. B. S. conceived the project, designed the study, supervised the research and wrote the manuscript. All authors have given approval to the final version of the manuscript.

Data availability

The data supporting this article have been included as part of the ESI.†

Conflicts of interest

There are no conflicts to declare.

Acknowledgements

We are thankful for grants CNS2022-135945, PID2022-142168NB-I00, TED2021-130946B-100, PID2019-107779GA-I00 provided by MICIU/AEI/10.13039/501100011033 and by "ERDF/EU" and by the "European Union NextGenerationEU/PRTR". We thank Anton Paar GmbH for allowing us to carry out the solid-state X-ray experiments at their facilities. Finally, we thank J. Cifre, F. Orvay, G. Martorell, and J. González from the Serveis Cientificotènics (SCT), UIB for technical support. B. S. is thankful to MICINN/AEI for the "Ramón-y-Cajal" fellowship (RYC-2017-21789). L. R. and P. X. are thankful to Govern de les Illes Balears for PhD fellowships (FPI_039_2020 and FPI_082_2022).

References

1 *Handbook of Liquid Crystals*, ed. J. W. Goodby, P. J. Collings, T. Kato, C. Tschierske, H. Gleeson and P. Raynes, Wiley-VCH, Weinheim, Germany, 2nd edn, 2014.
2 T. Wöhrle, I. Wurzbach, J. Kirres, A. Kostidou, N. Kapernaum, J. Litterscheidt, J. C. Haenle, P. Staffeld, A. Baro, F. Giesselmann and S. Laschat, Discotic Liquid Crystals, *Chem. Rev.*, 2016, **116**, 1139–1241.
3 M. Lehmann and P. Maier, Shape-Persistent, Sterically Crowded Star Mesogens: From Exceptional Columnar Dimer Stacks to Supermesogens, *Angew. Chem., Int. Ed.*, 2015, **54**, 9710–9714.
4 R. J. Bushby and K. Kawata, Liquid crystals that affected the world: discotic liquid crystals, *Liq. Cryst.*, 2011, **38**, 1415–1426.
5 S. Kumar, Functional Discotic Liquid Crystals, *Isr. J. Chem.*, 2012, **52**, 820–829.

6 C. Tschierske, Development of Structural Complexity by Liquid-Crystal Self-assembly, *Angew. Chem., Int. Ed.*, 2013, **52**, 8828–8878.
7 T. Kato, T. Yasuda, Y. Kamikawa and M. Yoshio, Self-assembly of functional columnar liquid crystals, *Chem. Commun.*, 2009, 729–739.
8 T. Kato, M. Yoshio, T. Ichikawa, B. Soberats, H. Ohno and M. Funahashi, Transport of ions and electrons in nanostructured liquid crystals, *Nat. Rev. Mater.*, 2017, **2**, 17001.
9 M.-S. Ho, B. E. Partridge, H.-J. Sun, D. Sahoo, P. Leowanawat, M. Peterca, R. Graf, H. W. Spiess, X. Zeng, G. Ungar, P. A. Heiney, C.-S. Hsu and V. Percec, Screening Libraries of Semifluorinated Arylene Bisimides to Discover and Predict Thermodynamically Controlled Helical Crystallization, *ACS Comb. Sci.*, 2016, **18**, 723–739.
10 H. K. Bisoyi and Q. Li, Liquid Crystals: Versatile Self-Organized Smart Soft Materials, *Chem. Rev.*, 2022, **122**, 4887–4926.
11 J. Uchida, B. Soberats, M. Gupta and T. Kato, Advanced Functional Liquid Crystals, *Adv. Mater.*, 2022, **34**, 2109063.
12 N. J. Hestand and F. C. Spano, Molecular Aggregate Photophysics beyond the Kasha Model: Novel Design Principles for Organic Materials, *Acc. Chem. Res.*, 2017, **50**, 341–350.
13 N. J. Hestand and F. C. Spano, Expanded Theory of H- and J-Molecular Aggregates: The Effects of Vibronic Coupling and Intermolecular Charge Transfer, *Chem. Rev.*, 2018, **118**, 7069–7163.
14 Y.-C. Lin, G.-S. Li, P.-J. Yu, E. Ercan and W.-C. Chen, Organic liquid crystals in optoelectronic device applications: Field-effect transistors, nonvolatile memory, and photovoltaics, *J. Chin. Chem. Soc.*, 2022, **69**, 1289–1304.
15 M. Funahashi, Nanostructured liquid-crystalline semiconductors - a new approach to soft matter electronics, *J. Mater. Chem. C*, 2014, **2**, 7451–7459.
16 E.-K. Fleischmann and R. Zentel, Liquid-Crystalline Ordering as a Concept in Materials Science: From Semiconductors to Stimuli-Responsive Devices, *Angew. Chem., Int. Ed.*, 2013, **52**, 8810–8827.
17 M. Kumar and S. Kumar, Liquid crystals in photovoltaics: a new generation of organic photovoltaics, *Polym. J.*, 2017, **49**, 85–111.
18 H.-W. Chen, J.-H. Lee, B.-Y. Lin, S. Chen and S.-T. Wu, Liquid crystal display and organic light-emitting diode display: present status and future perspectives, *Light: Sci. Appl.*, 2018, **7**, 17168–17168.
19 H. Iino, T. Usui and J.-I. Hanna, Liquid crystals for organic thin-film transistors, *Nat. Commun.*, 2015, **6**, 6828.
20 S. Herbst, B. Soberats, P. Leowanawat, M. Lehmann and F. Würthner, A Columnar Liquid-Crystal Phase Formed by Hydrogen-Bonded Perylene Bisimide J-Aggregates, *Angew. Chem., Int. Ed.*, 2017, **56**, 2162–2165.
21 S. Herbst, B. Soberats, P. Leowanawat, M. Stolte, M. Lehmann and F. Würthner, Self-assembly of multistranded perylene dye J-aggregates in columnar liquid-crystalline phases, *Nat. Commun.*, 2018, **9**, 2646.
22 M. Hecht, T. Schlossarek, S. Ghosh, Y. Tsutsui, A. Schmiedel, M. Holzapfel, M. Stolte, C. Lambert, S. Seki, M. Lehmann and F. Würthner, Nanoscale Columnar Bundles Based on Multistranded Core–Shell Liquid Crystals of Perylene Bisimide J-Aggregate Donor–Acceptor Dyads for Photoconductivity Devices with Enhanced Performance Through Macroscopic Alignment, *ACS Appl. Nano Mater.*, 2020, **3**, 10234–10245.
23 B. Soberats, M. Hecht and F. Würthner, Diketopyrrolopyrrole Columnar Liquid-Crystalline Assembly Directed by Quadruple Hydrogen Bonds, *Angew. Chem., Int. Ed.*, 2017, **56**, 10771–10774.
24 M. Hecht, B. Soberats, J. Zhu, V. Stepanenko, S. Agarwal, A. Greiner and F. Würthner, Anisotropic microfibres of a liquid-crystalline diketopyrrolopyrrole by self-assembly-assisted electrospinning, *Nanoscale Horiz.*, 2019, **4**, 169–174.
25 E. Castellanos, R. M. Gomila, R. Manha, G. Fernández, A. Frontera and B. Soberats, Columnar liquid-crystalline J-aggregates based on N-core-substituted naphthalene diimides, *J. Mater. Chem. C*, 2023, **11**, 10884–10892.
26 F. Würthner, T. E. Kaiser and C. R. Saha-Moller, J-Aggregates: From Serendipitous Discovery to Supramolecular Engineering of Functional Dye Materials, *Angew. Chem., Int. Ed.*, 2011, **50**, 3376–3410.
27 M. Hecht and F. Würthner, Supramolecularly Engineered J-Aggregates Based on Perylene Bisimide Dyes, *Acc. Chem. Res.*, 2021, **54**, 642–653.
28 F. C. Spano, The Spectral Signatures of Frenkel Polarons in H- and J-Aggregates, *Acc. Chem. Res.*, 2010, **43**, 429–439.
29 M. Dusel, S. Betzold, S. Brodbeck, S. Herbst, F. Würthner, D. Friedrich, B. Hecht, S. Höfling and C. P. Dietrich, Three-dimensional photonic confinement in imprinted liquid crystalline pillar microcavities, *Appl. Phys. Lett.*, 2017, **110**, 201113.
30 M. Hecht, T. Schlossarek, M. Stolte, M. Lehmann and F. Würthner, Photoconductive Core–Shell Liquid-Crystals of a Perylene Bisimide J-Aggregate Donor–Acceptor Dyad, *Angew. Chem., Int. Ed.*, 2019, **58**, 12979–12983.
31 E. D. Głowacki, M. Irimia-Vladu, S. Bauer and N. S. Sariciftci, Hydrogen-bonds in molecular solids–from biological systems to organic electronics, *J. Mater. Chem. B*, 2013, **1**, 3742–3753.
32 W. Cui, J. Yuen and F. Wudl, Benzodipyrrolidones and their polymers, *Macromolecules*, 2011, **44**, 7869–7873.
33 Z. Deng, T. Ai, R. Li, W. Yuan, K. Zhang, H. Du and H. Zhang, Conjugated Polymers Containing Building Blocks 1,3,4,6-Tetraarylpyrrolo[3,2-b]pyrrole-2,5-dione (isoDPP), Benzodipyrrolidone (BDP) or Naphthodipyrrolidone (NDP): A Review, *Polymers*, 2019, **11**, 1683.
34 K. C. Lee, W.-T. Park, Y.-Y. Noh and C. Yang, Benzodipyrrolidone (BDP)-Based Polymer Semiconductors Containing a Series of Chalcogen Atoms: Comprehensive Investigation of the Effect of Heteroaromatic Blocks on

Intrinsic Semiconducting Properties, *ACS Appl. Mater. Interfaces*, 2014, **6**, 4872–4882.

35 J. Deng, W. Zheng, Y. Wang, M. Cheng, Q. Jin, Y. Ke, Z. Zheng, R. A. J. Janssen, L. Li, M. Liu, H. I. Wang and M. Li, Polymorph-Dependent Multi-Level Supramolecular Self-Assembly and Local Charge Transport of a Conjugated Polymer in Solution and Solid States, *Adv. Energy Mater.*, 2024, 2402778.

36 H. Zhang, K. Yang, Y.-M. Chen, R. Bhatta, M. Tsige, S. Z. D. Cheng and Y. Zhu, Polymers Based on Benzodipyrrolidone and Naphthodipyrrolidone with Latent Hydrogen-Bonding on the Main Chain, *Macromol. Chem. Phys.*, 2017, **218**, 1600617.

37 Y. Zhou, W. Zhang and G. Yu, Recent structural evolution of lactam- and imide-functionalized polymers applied in organic field-effect transistors and organic solar cells, *Chem. Sci.*, 2021, **12**, 6844–6878.

38 Z. Deng, X. Hao, P. Zhang, L. Li, X. Yuan, T. Ai, W. Bao and K. Kou, Donor-acceptor-donor molecules based on diketopyrrolopyrrole, benzodipyrrolidone and naphthodipyrrolidone: Organic crystal field-effect transistors, *Dyes Pigm.*, 2019, **162**, 883–887.

39 N. Gospodinova and E. Tomšík, Hydrogen-bonding versus π–π stacking in the design of organic semiconductors: From dyes to oligomers, *Prog. Polym. Sci.*, 2015, **43**, 33–47.

40 T. Xiao, L. Xu, J. Götz, M. Cheng, F. Würthner, J. Gu, X. Feng, Z.-Y. Li, X.-Q. Sun and L. Wang, Supramolecular polymerization and cyclization of dioxynaphthalene motif bridged bifunctional UPys: minor variations in the molecular skeleton and drastic differences in self-assembly, *Mater. Chem. Front.*, 2019, **3**, 2738–2745.

41 T. Xiao, L. Xu, J. Wang, Z.-Y. Li, X.-Q. Sun and L. Wang, Biomimetic folding of small organic molecules driven by multiple non-covalent interactions, *Org. Chem. Front.*, 2019, **6**, 936–941.

42 T. F. A. De Greef, M. M. J. Smulders, M. Wolffs, A. P. H. J. Schenning, R. P. Sijbesma and E. W. Meijer, Supramolecular Polymerization, *Chem. Rev.*, 2009, **109**, 5687–5754.

43 M. Hartlieb, E. D. H. Mansfield and S. Perrier, A guide to supramolecular polymerizations, *Polym. Chem.*, 2020, **11**, 1083–1110.

44 G. Ghosh, P. Dey and S. Ghosh, Controlled supramolecular polymerization of π-systems, *Chem. Commun.*, 2020, **56**, 6757–6769.

45 M. M. J. Smulders, M. M. L. Nieuwenhuizen, T. F. A. de Greef, P. van der Schoot, A. P. H. J. Schenning and E. W. Meijer, How to Distinguish Isodesmic from Cooperative Supramolecular Polymerisation, *Chem. – Eur. J.*, 2010, **16**, 362–367.

46 L. Herkert, J. Droste, K. K. Kartha, P. A. Korevaar, T. F. A. de Greef, M. R. Hansen and G. Fernández, Pathway Control in Cooperative vs. Anti-Cooperative Supramolecular Polymers, *Angew. Chem., Int. Ed.*, 2019, **58**, 11344–11349.

47 T. E. Kaiser, H. Wang, V. Stepanenko and F. Würthner, Supramolecular construction of fluorescent J-aggregates based on hydrogen-bonded perylene dyes, *Angew. Chem., Int. Ed.*, 2007, **46**, 5541–5544.

48 H. M. M. ten Eikelder, A. J. Markvoort, T. F. A. de Greef and P. A. J. Hilbers, An Equilibrium Model for Chiral Amplification in Supramolecular Polymers, *J. Phys. Chem. B*, 2012, **116**, 5291–5301.

49 P. A. Korevaar, C. Schaefer, T. F. A. de Greef and E. W. Meijer, Controlling Chemical Self-Assembly by Solvent-Dependent Dynamics, *J. Am. Chem. Soc.*, 2012, **134**, 13482–13491.

50 F. Orvay, J. Cerda, C. Rotger, E. Orti, J. Arago, A. Costa and B. Soberats, Influence of the Z/E Isomerism on the Pathway Complexity of a Squaramide-Based Macrocycle, *Small*, 2021, **17**, e2006133.

51 F. Nunes da Silva, H. Marchi Luciano, C. H. Stadtlober, G. Farias, F. Durola, J. Eccher, I. H. Bechtold, H. Bock, H. Gallardo and A. A. Vieira, Columnar Liquid Crystalline Glasses by Combining Configurational Flexibility with Moderate Deviation from Planarity: Extended Triaryltriazines, *Chem. – Eur. J.*, 2023, **29**, e202203604.

52 N. Godbert, A. Crispini, M. Ghedini, M. Carini, F. Chiaravalloti and A. Ferrise, LCDiXRay: a user-friendly program for powder diffraction indexing of columnar liquid crystals, *J. Appl. Crystallogr.*, 2014, **47**, 668–679.

53 M. Lambov, N. Hensiek, A.-C. Pöppler and M. Lehmann, Columnar Liquid Crystals from Star-Shaped Conjugated Mesogens as Nano-Reservoirs for Small Acceptors, *ChemPlusChem*, 2020, **85**, 2219–2229.

54 L. Rubert, M. F. Islam, A. B. Greytak, R. Prakash, M. D. Smith, R. M. Gomila, A. Frontera, L. S. Shimizu and B. Soberats, Two-Dimensional Supramolecular Polymerization of a Bis-Urea Macrocycle into a Brick-Like Hydrogen-Bonded Network, *Angew. Chem., Int. Ed.*, 2023, **62**, e202312223.

